

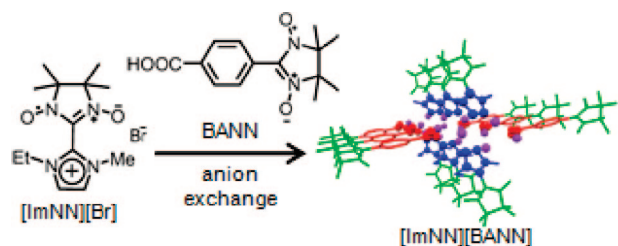
Molecular Structure and Magnetic Properties of 1-Ethyl-2-(1-oxy-3-oxo-4,4,5,5-tetramethylimidazolin-2-yl)-3-methylimidazolium Arylcarboxylates and Other Salts

Hiroyuki Hayashi, Satoru Karasawa, and Noboru Koga*

Graduate School of Pharmaceutical Sciences, Kyushu University,
3-1-1 Maidashi, Higashi-ku, Fukuoka, 812-8582, Japan

koga@fc.phar.kyushu-u.ac.jp

Received July 30, 2008



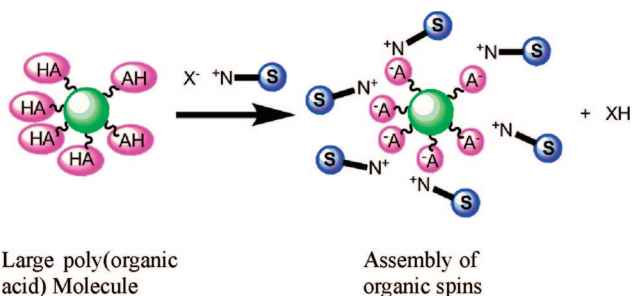
1-Ethyl-2-(1-oxy-3-oxo-4,4,5,5-tetramethylimidazolin-2-yl)-3-methylimidazolium bromide, $[\text{EMINN}]^+[\text{Br}]^-$, carrying nitronyl nitroxide (NN) in the cation unit, was prepared as a parent molecule and converted to seven salts, $[\text{EMINN}]^+[\text{X}]^-$ ($\text{X} = \text{I}$, TFSI (bis(trifluoromethanesulfonyl)imide), BPh_4 (tetraphenylborate), $[\text{EMINN}]^+_{1-3}[\text{BA}_{1-3}]^{(1-3)-}$; BA_1 (benzoic acid), BA_2 (terephthalic acid), and BA_3 (trimesic acid), and $[\text{EMINN}]^+[\text{BANN}]^-$; BANN (4-NN-benzoic acid)), by the ion-exchange reaction. The molecular structure of the cation units for all salts revealed by X-ray crystallography is similar, where the dihedral angles between the imidazolium ring and the NN planes are $51\text{--}58^\circ$. In the crystal structure, $[\text{EMINN}]^+[\text{X}]^-$ ($\text{X} = \text{Br}$, I , TFSI, and BPh_4) formed head-to-tail dimers, while the uniquely shaped dimers consisting of two $[\text{EMINN}]^+[\text{carboxylate}]^-$ units were connected by the hydrogen bonding of water molecules to form a tape structure for $[\text{EMINN}]^+[\text{BANN}]^-$ and 2D sheet structure for $[\text{EMINN}]^+_{2}[\text{BA}_2]^{2-}$ and $[\text{EMINN}]^+_{3}[\text{BA}_3]^{3-}$. In the crystalline state, $[\text{EMINN}]^+[\text{X}]^-$ showed behavior typical of a paramagnetic species with $S = 1/2$. The $\chi_{\text{mol}}T$ vs T plot for $[\text{EMINN}]^+[\text{BANN}]^-$ was analyzed using a four-spin model to give $J_1/k_B = -0.27$ and $J_2/k_B = -0.16$ K. The plots for $[\text{EMINN}]^+_{2}[\text{BA}_2]^{2-}$ and $[\text{EMINN}]^+_{3}[\text{BA}_3]^{3-}$ were analyzed using an antiferromagnetic chain model to give $J/k_B = -62.1$ and -86.5 K, respectively. In aqueous solution, on the other hand, the ESR spectra for all salts showed similar five-line signals due to the isolated NN moiety. The relaxivities (r_1 and r_2 ; 25°C , 0.59 T, and 25 MHz) for $[\text{EMINN}]^+[\text{Br}]^-$, $[\text{EMINN}]^+[\text{BA}]^-$, $[\text{EMINN}]^+[\text{BANN}]^-$, $[\text{EMINN}]^+_{2}[\text{BA}_2]^{2-}$, and $[\text{EMINN}]^+_{3}[\text{BA}_3]^{3-}$, are $r_1 = 0.13, 0.14, 0.32, 0.26,$ and 0.40 and $r_2 = 0.17, 0.13, 0.31, 0.30,$ and 0.46 $\text{mM}^{-1} \text{s}^{-1}$, respectively.

Introduction

Stable organic radicals have been used as a spin source for organic ferromagnets¹ and heterospin single-molecular magnets² in the field of molecule-based magnets.³ In the clinical and biological fields, on the other hand, they have long been known

as reagents of spin labeling and spin trapping,⁴ spin probes for reactive oxygen and nitrogen species⁵ (ROS and RNS, respectively), and candidates for magnetic resonance imaging (MRI) contrast agents.⁶ MRI, which has made it possible to image deep from the surface, has become a powerful tool for diagnosis in

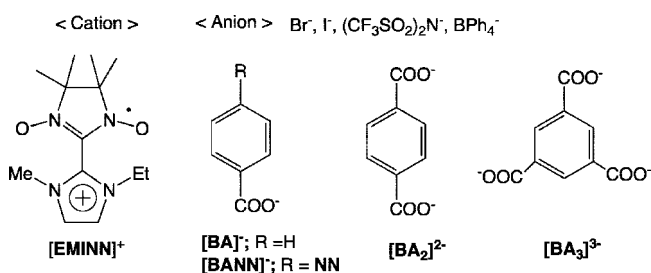
SCHEME 1. Strategy for Assembling the Organic Spin in an Organic Salt System



the clinical field. In MRI, agents used to enhance the contrast are paramagnetic or superparamagnetic species. Recently, for the construction of a new type of contrast agent, large molecules^{7,8} such as polymers⁹ including dendrimers¹⁰ and assemblies¹¹ having stable radicals and chelating metal ions (especially Gd(III) ion) were intensively investigated in vitro and in vivo. In these studies, the spin sources were attached by a covalent bond. This time, we considered introducing many organic spins into a large molecule with an ionic bond. The combination of a poly(organic acid) of large molecular size and an organic cation carrying a stable organic spin was expected to readily assemble the organic spin by a simple procedure, the ion-exchange reaction (Scheme 1). Furthermore, various macromolecules such as proteins and DNA with anionic groups exist in vivo and are allowed to be targeted.

To understand the ion-pair molecules in detail, small anionic molecules were employed and the local structure, cation–anion interaction, and the magnetic properties of the ion-pair molecules were investigated in the crystalline state and in solution. An ionic liquid (IL), a class of organic salt, was selected as the main framework. In ILs,¹² the ion-exchange reaction of the

counterion and the cation–anion interactions leading to their unique physical properties have been intensively investigated.¹³ An ionic molecule, 1-ethyl-2-(1-oxy-3-oxo-4,4,5,5-tetramethylimidazolium-2-yl)-3-methylimidazolium bromide, [EMINN]⁺[Br][−], where nitronyl nitroxide (NN) and 1,3-dialkylimidazolium cation are known as a stable radical and an IL molecule, respectively, was prepared as a parent radical salt. In addition, [EMINN]⁺[X][−] (X = I, TFSI (bis(trifluoromethanesulfonyl)imide), and BPh₄ (tetraphenylborate)) having different sized anions were prepared. To confirm the cation–anion interaction with organic acid, arylcarboxylic acids, [BA_{1–3}]; BA₁ = benzoic acid, BA₂ = terephthalic acid, and BA₃ = trimesic acid, were employed, and anion-exchange reactions with them were carried out. The bromide anion in [EMINN]⁺[Br][−] was replaced with [BA_{1–3}]^{(1–3)−} via [EMINN]⁺[OH][−] to afford [EMINN]⁺[BA_{1–3}]^{(1–3)−}. An analogous salt, [EMINN]⁺[BANN][−], which has NN radicals in both the cation and anion units, was also prepared by using 4-(nitronyl nitroxide)benzoic acid, [BANN], in a similar manner.



The molecular structure and magnetic properties of [EMINN]⁺[X][−] (X = Br, I, TFSI, and BPh₄), [EMINN]⁺[BANN][−], and [EMINN]⁺[BA_{2–3}]^{(2–3)−} were investigated in the crystalline state and in solution. In addition, the water–proton relaxation time in the presence of these salts was measured in water, and relaxivity (*r*₁ and *r*₂; longitudinal and transverse relaxivity, respectively) was evaluated.

Results and Discussion

Preparation of 1-Ethyl-2-(1-oxy-3-oxo-4, 4, 5, 5-tetramethylimidazolium-2-yl)-3-methylimidazolium bromide and Its I[−], TFSI[−], BPh₄[−], and Arylcarboxylate Salts. The routes for the preparation of the parent molecule, [EMINN]⁺[Br][−], and [EMINN]⁺[X][−] (X = I, TFSI, and BPh₄), [EMINN]⁺[BANN][−], [EMINN]⁺[BA][−], [EMINN]⁺[BA₂]^{2−}, and [EMINN]⁺[BA₃]^{3−} are shown in Scheme 2.

1-Methyl-2-(1-oxy-3-oxo-4,4,5,5-tetramethylimidazolium-2-yl)imidazole, MINN, was prepared by the standard procedure of the reaction of the corresponding 2-formylimidazole with a

(1) (a) Rajca, A.; Wongsriratanakul, J.; Rajca, S. *J. Am. Chem. Soc.* **2004**, *126*, 6608–6626. (b) Kinoshita, M.; Turek, P.; Tamura, M.; Nozawa, K.; Shiomi, D.; Nakazawa, Y.; Ishikawa, M.; Takahashi, M.; Awaga, K.; Inabe, T.; Maruyama, Y. *Chem. Lett.* **1991**, 1225–1228. (c) Chiarelli, R.; Novak, M. A.; Rassat, A.; Tholence, J. L. *Nature* **1993**, *363*, 147–149.

(2) (a) Koga, N.; Karasawa, S. *Bull. Chem. Soc. Jpn.* **2005**, *78*, 1384–1400. (b) Karasawa, S.; Zhou, G.; Morikawa, H.; Koga, N. *J. Am. Chem. Soc.* **2003**, *125*, 13676–13677. (c) Kanegawa, S.; Karasawa, S.; Nakano, M.; Koga, N. *Bull. Chem. Soc. Jpn.* **2006**, *79*, 1372–1382. (d) Kanegawa, S.; Karasawa, S.; Nakano, M.; Koga, N. *Chem. Commun.* **2004**, 1750–1751. (e) Kanegawa, S.; Karasawa, S.; Maeyama, M.; Nakano, M.; Koga, N. *J. Am. Chem. Soc.* **2008**, *130*, 3079–3094.

(3) (a) Kahn, O. *Molecular Magnetism*; Wiley-VCH: New York, 1993. (b) Kahn, O. *Nature* **1995**, *378*, 667–668. (c) Gatteschi, D. *Adv. Mater.* **1994**, *6*, 635–645. (d) Miller, J. S.; Epstein, A. J.; Reiff, W. M. *Chem. Rev.* **1988**, *88*, 201–220. (e) Ohba, M.; Okawa, H. *Coord. Chem. Rev.* **2000**, *198*, 313–328. (f) Sato, O.; Iyoda, T.; Fujishima, A.; Hashimoto, K. *Science* **1996**, *272*, 704–705.

(4) (a) Kaneko, T.; Aso, M.; Koga, N.; Suemune, H. *Org. Lett.* **2005**, *7*, 303–306. (b) Cataldo, L.; Dutan, C.; Misra, S. K.; Loss, S.; Grutzmacher, H.; Geoffroy, M. *Chem.—Eur. J.* **2005**, *11*, 3463–3468. (c) Inbaraj, J. J.; Cardon, T. B.; Laryukhin, M.; Grosser, S. M.; Lorigan, G. A. *J. Am. Chem. Soc.* **2006**, *128*, 9549–9554.

(5) (a) Utsumi, H.; Yasukawa, K.; Soeda, T.; Yamada, K.; Shigemi, R.; Yao, T.; Tsuneyoshi, M. *J. Pharmacol. Exp. Ther.* **2006**, *317*, 228–235. (b) Saito, K.; Takeshita, K.; Anzai, K.; Ozawa, T. *Free Radic. Biol. Med.* **2004**, *36*, 517–525. (c) Murrant, C. L.; Reid, M. B. *Microsc. Res. Tech.* **2001**, *55*, 236–248.

(6) (a) Brasch, R. C.; London, D. A.; Wesbey, G. E.; Tozer, T. N.; Nitecki, D. E.; Williams, R. D.; Doemeny, J.; Tuck, L. D.; Lallemand, D. P. *Radiology* **1983**, *147*, 773–779. (b) Bacic, G.; Liu, K. J.; Goda, F.; Hoopes, P. J.; Rosen, G. M.; Swarts, H. M. *Magn. Reson. Med.* **1997**, *37*, 764–768. (c) Huang, Y.; Nan, A.; Rosen, G. M.; Winalski, C. S.; Schneider, E.; Tsai, P.; Ghandehari, H. *Macromol. Biosci.* **2003**, *3*, 647–652.

(7) (a) Bloembergen, N.; Purcell, E. M.; Pound, R. V. *Phys. Rev.* **1948**, *73*, 679–712. (b) Sharp, R. R. *J. Chem. Phys.* **1993**, *98*, 2507–2515. (c) Korb, J. P.; Diakova, G.; Bryant, R. G. *J. Chem. Phys.* **2006**, *124*, 134910. (d) Maliakal, A. J.; Turro, N. J.; Bosman, A. W.; Cornel, J.; Meijer, E. W. *J. Phys. Chem. A* **2003**, *107*, 8467–8475.

(8) Maeda, H. *Adv. Enzyme Regul.* **2001**, *41*, 189–207.

(9) (a) Allen, M. J.; Raines, R. T.; Kiessling, L. L. *J. Am. Chem. Soc.* **2006**, *128*, 6534–6535. (b) Toth, E.; Helm, L.; Kellar, K. E.; Merbach, A. E. *Chem.—Eur. J.* **1999**, *5*, 1202–1211.

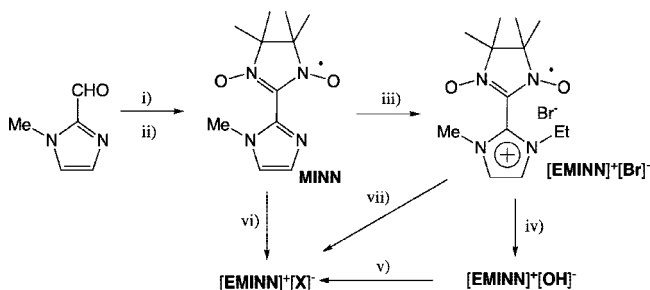
(10) (a) Winalski, C. S.; Shortkroff, S.; Mulkern, R. V.; Schneider, E.; Rosen, G. M. *Magn. Reson. Med.* **2002**, *48*, 965–972. (b) Livramento, J. B.; Sour, A.; Borel, A.; Merbach, A. E.; Toth, E. *Chem.—Eur. J.* **2006**, *12*, 989–1003.

(11) Gianolio, E.; Giovenzana, G. B.; Longo, D.; Longo, I.; Menegotto, I.; Aime, S. *Chem.—Eur. J.* **2007**, *13*, 5785–5797.

(12) (a) Morris, R. E. *Angew. Chem., Int. Ed.* **2008**, *47*, 442–444. (b) Zayed, F.; Greiner, L.; Schulz, P. S.; Lapkin, A.; Leitner, W. *Chem. Commun.* **2008**, 79–81. (c) Migowski, P.; Dupont, J. *Chem.—Eur. J.* **2007**, *13*, 32–39.

(13) (a) Li, H.; Boatz, J. A.; Gordon, M. S. *J. Am. Chem. Soc.* **2008**, *130*, 392–393. (b) Kulkarni, P. S.; Branco, L. C.; Crespo, J. G.; Nunes, M. C.; Raymundo, A.; Afonso, C. A. M. *Chem.—Eur. J.* **2007**, *13*, 8478–8488. (c) Fraser, K. J.; Izgorodina, E. I.; Forsyth, M.; Scott, J. L.; MacFarlane, D. R. *Chem. Commun.* **2007**, 3817–3819.

SCHEME 2. Preparation of [EMINN]⁺[X]⁻; X = Br, I, TFSI, and BPh₄, [EMINN]⁺[BA]⁻, [EMINN]⁺[BANN]⁻, [EMINN]⁺₂[BA₂]²⁻, and [EMINN]⁺₃[BA₃]³⁻^a



^a Key: (i) 2,3-bis(hydroxyamino)-2,3-dimethylbutane sulfate, K₂CO₃, H₂O, rt; (ii) PbO₂, CH₂Cl₂, rt; (iii) ethyl bromide, toluene, reflux; (iv) anion-exchange resin; (v) arylcarboxylic acids; (vi) ethyl iodide, CHCl₃, reflux; (vii) LiTFSI or NaBPh₄.

hydroxylamine and oxidation with PbO₂ followed by the *N*-alkylation reaction of MINN with ethyl bromide. 1-Methyl-2-(1-oxy-3-oxo-4,4,5,5-tetramethylimidazol-2-yl)-3-ethylimidazolium bromide, [EMINN]⁺[Br]⁻, was obtained as a parent radical in good yield and was stable at ambient temperature. To investigate the effect of the bulkiness of the counteranion, analogous salts, [EMINN]⁺[X]⁻ (X = I, TFSI, and BPh₄) were also prepared: [EMINN]⁺[I]⁻ by a procedure similar to that for the bromide salt and [EMINN]⁺[TFSI]⁻ and [EMINN]⁺[BPh₄]⁻ by a direct exchange reaction with Li⁺TFSI⁻ and Na⁺BPh₄⁻, respectively. The exchange reactions of bromide with arylcarboxylate were carried out by the procedure reported previously.¹⁴ Bromide anion was changed to hydroxide anion by passing it through an anion-exchange column. Because the [EMINN]⁺[OH]⁻ obtained was relatively unstable, the aqueous solution was used without isolation. The resulting [EMINN]⁺[OH]⁻ solution was mixed with a water solution of arylcarboxylic acid, [BA_{*n*}]^{*n-*}; *n* = 1–3 and [BANN], to afford [EMINN]⁺_{*n*}[BA_{*n*}]^{*n-*} and [EMINN]⁺[BANN]⁻, respectively.

All salts were obtained as blue colored powders with relatively high melting points (mp > 150 °C) and, except for [EMINN]⁺[TFSI]⁻ and [EMINN]⁺[BPh₄]⁻, dissolved well in water. [EMINN]⁺[TFSI]⁻ and [EMINN]⁺[BPh₄]⁻ were insoluble in water. All crude salts were recrystallized from the mixed solvent to afford single crystals as blue plates. The crystals of arylcarboxylate salts were relatively hygroscopic, while those of [EMINN]⁺[X]⁻ (X = Br⁻, I⁻, TFSI⁻, and BPh₄⁻) were stable at ambient condition. Therefore, X-ray crystallography for [EMINN]⁺[BANN]⁻, [EMINN]⁺₂[BA₂]²⁻, and [EMINN]⁺₃[BA₃]³⁻ was carried out using the single crystals immediately after taking out of the solvent for the recrystallization. However, that for [EMINN]⁺[BA]⁻ failed using a similar procedure. The crystal was extremely hygroscopic and gradually dissolved in moisture.

X-ray Crystallography. The molecular and crystal structures of seven salts, [EMINN]⁺[X]⁻ (X = Br, I, TFSI, and BPh₄, [EMINN]⁺[BANN]⁻, [EMINN]⁺₂[BA₂]²⁻, and [EMINN]⁺₃[BA₃]³⁻), were investigated by X-ray crystallography. In the molecular structure, the cation units of all these salts are similar. In the cation unit, both planes of the imidazolium ring and the NN plane are extensively twisted by ethyl and methyl substituents of the imidazolium ring, and the dihedral angles (NN–Im) between the imidazolium ring and the NN plane are 51–58°.

(14) Fukumoto, K.; Yoshizawa, M.; Ohno, H. *J. Am. Chem. Soc.* **2005**, *127*, 2398–2399.

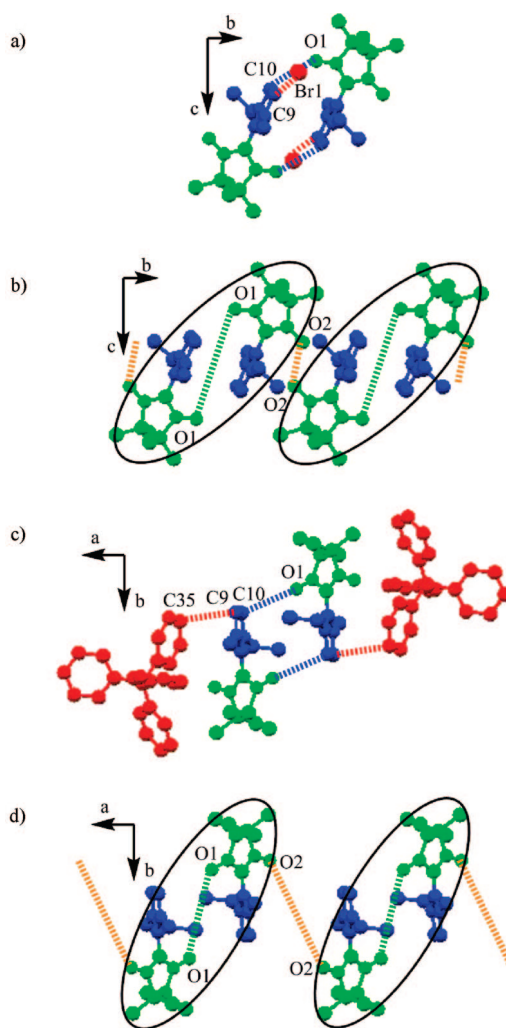


FIGURE 1. Dimer structure of (a) [EMINN]⁺[Br]⁻ and (c) [EMINN]⁺[BPh₄]⁻ and packing diagram for (b) [EMINN]⁺[Br]⁻ and (d) [EMINN]⁺[BPh₄]⁻ with a ball-stick model (color code: NN moiety, green; Im cation, blue; anion, red). In (a) and (c), the short O(NN)–C(Im) and anion–C(Im) contacts within the dimers are indicated by the blue and red dashed lines, respectively. In (b) and (d), the anion units are omitted for the sake of clarity, and the short NO–NO contacts within and between dimers are indicated by the green and orange dashed lines, respectively. Each dimer is indicated by a circle.

In the cation–anion pair, carbon C9 or C10 of the imidazolium ring, where the cation was delocalized, is close to the atom of the anion unit. Furthermore, it is noted that the cation–anion pairs for all salts exist as the dimer in the crystal lattice. The crystal structure for [EMINN]⁺[X]⁻ (X = Br, I, TFSI, and BPh₄) strongly depends on the size of anion unit. In arylcarboxylate salts, the hydrogen bonding of the water molecules contained as crystal solvents is important to the formation of the anion chain or sheet structure in the crystal lattice.

(A) [EMINN]⁺[X]⁻ (X = Br, I, TFSI, and BPh₄). The molecular and crystal structures are shown in Figure 1 for [EMINN]⁺[Br]⁻ and [EMINN]⁺[BPh₄]⁻ and in Figure S2 (Supporting Information) for [EMINN]⁺[I]⁻ and [EMINN]⁺[TFSI]⁻. The dihedral angles (NN–Im; O1N1C1N2O2–C8C9C10) are 54.98 and 57.71° for [EMINN]⁺[Br]⁻ and [EMINN]⁺[BPh₄]⁻, respectively. The anion units are located near carbon C9 of the imidazolium cation at a distance of 3.65 (C9–Br1) for [EMINN]⁺[Br]⁻ and 3.25 Å (C9–C35) for [EMINN]⁺[BPh₄]⁻. In the crystal packing, the two molecules formed a head-to-tail

TABLE 1. Selected Dihedral Angles and Distances for [EMINN]⁺[Br]⁻, [EMINN]⁺[I]⁻, [EMINN]⁺[TFSI]⁻, and [EMINN]⁺[BPh₄]^{-a}

[EMINN] ⁺ [Br] ⁻		[EMINN] ⁺ [I] ⁻		[EMINN] ⁺ [TFSI] ⁻		[EMINN] ⁺ [BPh ₄] ⁻	
Dihedral Angles (deg) between the NN and the Imidazolium Planes							
O1N1C1N2O2–C8C9C10	54.98	O1N1C1N2O2–C8C9C10	55.10	O1N1C1N2O2–C8C9C10	54.49	O1N1C1N2O2–C8C9C10	57.71
Shortest Distance (Å) between the Cation and the Anion							
C9–Br1	3.65	C9–I1	3.87	C10–O5	3.13	C9–C35	3.25
Shortest Distance (Å) between the Cation Units within the Dimer							
O1–C9 O1–C10	3.06	O1–C9	3.08	O1–N3	2.98	O1–C10	3.61
Distances (Å) between the NN Centers							
within the dimer		within the dimer		within the dimer		within the dimer	
O1–O1'	6.61 (6.94)	O1–O1'	6.57(6.95)	O1–O1'	3.38 (4.22)	O1–O1'	6.40 (6.69)
between the dimers		between the dimers		between the dimers		between the dimers	
O2–O2'	3.99 (4.32)	O2–O2'	4.05 (4.37)	O2–O2'	6.70 (7.32)	O2–O2'	6.85 (7.39)

^a Numbers in parentheses are the distances between the middle of the NO bonds.

dimer via imidazolium–NN interaction. Within the dimer for [EMINN]⁺[Br]⁻ and [EMINN]⁺[BPh₄]⁻, the shortest distances between the cation units are 3.06 and 3.61 Å for those (O1–C10) between the oxygen O1 of NN and the carbon C10 of imidazolium, respectively, and those between the NN centers (O1–O1') are 6.61 and 6.40 Å, respectively. The distances between the dimers in these salts depend on the size of the counteranion (Figure 1). The NO–NO distance (O2–O2') between the dimers is 3.99 and 6.85 Å for [EMINN]⁺[Br]⁻ and [EMINN]⁺[BPh₄]⁻, respectively. The corresponding angles and distances for [EMINN]⁺[I]⁻ and [EMINN]⁺[TFSI]⁻ are summarized in Table 1.

The NO–NO distances suggest that the radical centers for [EMINN]⁺[Br]⁻ and [EMINN]⁺[I]⁻ magnetically interact not within the dimer but between the dimers, while those for [EMINN]⁺[TFSI]⁻ might interact within the dimer, not between the dimers, and those for [EMINN]⁺[BPh₄]⁻ are separated enough that their magnetic interaction may be insignificant.

(B) [EMINN]⁺[BANN]⁻, [EMINN]⁺₂[BA₂]²⁻, and [EMINN]⁺₃[BA₃]³⁻. The single crystals for [EMINN]⁺[BANN]⁻, [EMINN]⁺₂[BA₂]²⁻, and [EMINN]⁺₃[BA₃]³⁻ have 8, 4, and 40 water molecules, respectively, in a unit cell, findings which were supported by the results of the elementary analysis. In the molecular structure of [EMINN]⁺[BANN]⁻, the dihedral angles for NN–Im (O1N1C1N2O2–C8C9C10) and NN–Ph (O3N5C14N6O4–C21C23C25) are 57.98 and 29.01°, respectively. The latter value is consistent with that reported previously.¹⁵ [EMINN]⁺₂[BA₂]²⁻ consists of one anion unit and two cation units with a dihedral angle (NN–Im) of 50.54°. The unit cell of [EMINN]⁺₃[BA₃]³⁻ contains two nonsymmetric equivalent molecules marked by A and B on the benzene ring of trimesic acid in Figure 4, and each molecule has three cation units with different dihedral angles (NN–Im = 56.00, 54.14, and 51.31° for A and 54.96, 53.40, and 50.59° for B).

In these three salts, a unique local structure of the imidazolium–carboxylate was observed. Each imidazolium–carboxylate pair forms a dimer. As illustrated in Figure 2, two carboxylates in anion units paired with the imidazolium cations in an L shape are linked by the hydrogen bond of the water molecules to form the ion-pair dimer D.

The structure of the dimer D part in [EMINN]⁺[BANN]⁻, [EMINN]⁺₂[BA₂]²⁻, and [EMINN]⁺₃[BA₃]³⁻ is shown in Figure 3. In the dimer D of [EMINN]⁺[BANN]⁻, the carbon atoms at

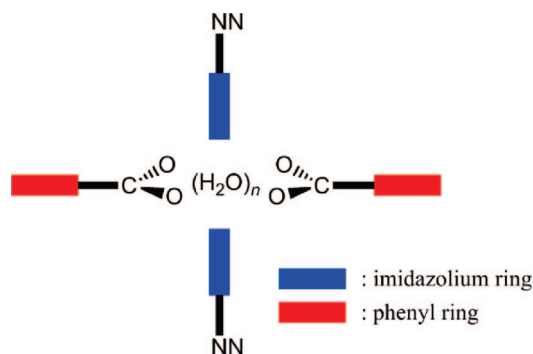


FIGURE 2. Illustration of the structure of dimer D.

C9 and C10 of imidazolium cation rings bridge the oxygen (O6) of the carboxylate and one (O7) of the water molecules, in which the distance of O6–C10 and O7–C9 are 3.04 and 3.23 Å, respectively (Figure 3a). On the other hand, [EMINN]⁺₂[BA₂]²⁻ and [EMINN]⁺₃[BA₃]³⁻ have two and three imidazolium–carboxylate pairs, respectively, and thus the formation of dimer D produces a 1D chain for [EMINN]⁺₂[BA₂]²⁻ and a 2D sheet structures for [EMINN]⁺₃[BA₃]³⁻. In [EMINN]⁺₂[BA₂]²⁻, the imidazolium–carboxylate pairs, in which the distance between C10 of imidazolium and O4 of carboxylate is 3.49 Å, were connected by a water molecule to form 1D chain. Similarly, in [EMINN]⁺₃[BA₃]³⁻, the dimer D structure was observed at each carboxylate unit of trimesic acid.

Furthermore, the carboxylate anion units produce the tape structure for [BANN]⁻ and sheet structures for [BA₂]²⁻ and [BA₃]³⁻ through the hydrogen bond of water molecules contained in the crystal. The only hydrogen bond patterns of water molecules with the arylcarboxylate units were extracted and are shown in Figure 4. In the observed hydrogen bond patterns, interestingly, the structures of the ideal water cluster can be found. In [EMINN]⁺[BANN]⁻, a ring structure (tetramer) consisting of four water molecules was observed. According to the calculation of the tetramer of water molecules reported in the literature, it is structure symbolized by R4¹⁶ is the 2DD2AA structure consisting of two hydrogen-donor and two hydrogen-acceptor water molecules in the hydrogen bond and its Boltzmann distribution percentage was zero.¹⁷ The 2DD2AA structure has very unfavorable dipole–dipole interactions, as the dipole

(16) Mascial, M.; Infantes, L.; Chisholm, J. *Angew. Chem., Int. Ed.* **2006**, *45*, 32–36.

(17) Day, M. B.; Kirschner, K. N.; Shields, G. C. *J. Phys. Chem. A* **2005**, *109*, 6773.

(15) Turek, P.; Nozawa, K.; Shiomi, D.; Awaga, K.; Inabe, T.; Maruyama, Y.; Kinoshita, M. *Chem. Phys. Lett.* **1991**, *180*, 327–331.

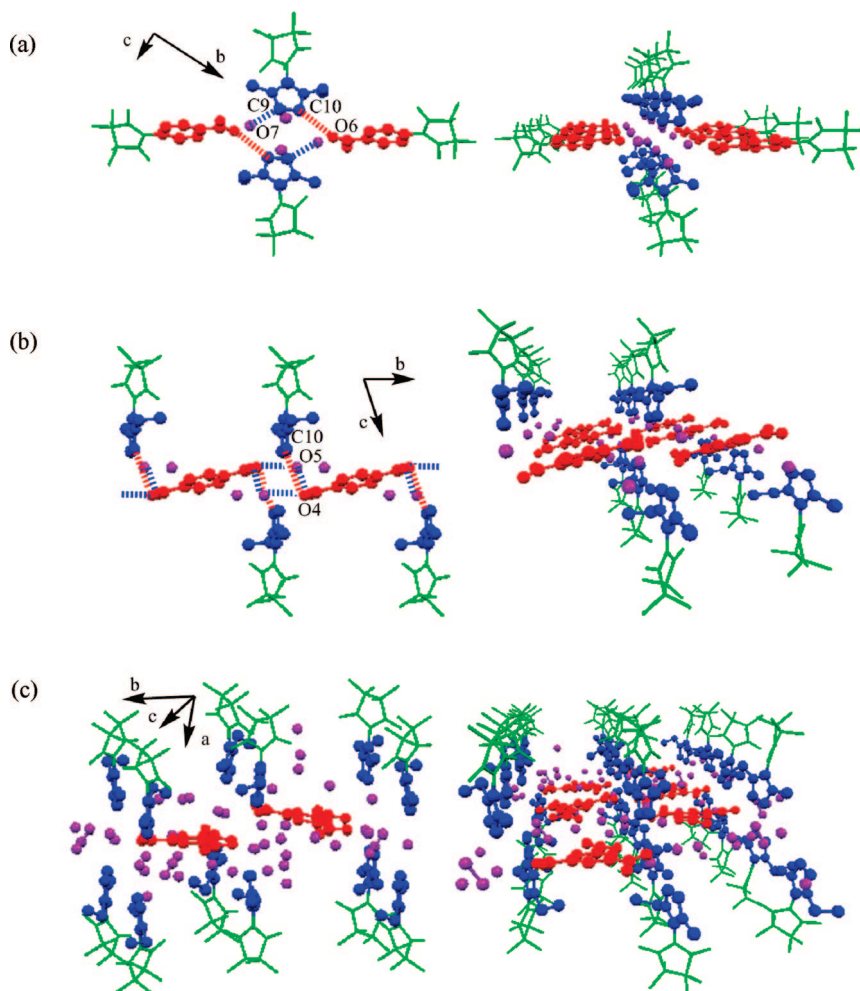


FIGURE 3. Crystal packing of dimer Ds for (a) $[\text{EMINN}]^+[\text{BANN}]^-$, (b) $[\text{EMINN}]_2^+[\text{BA}_2]^{2-}$ and (c) $[\text{EMINN}]_3^+[\text{BA}_3]^{3-}$ shown with a ball-stick model (color: NN moiety, green; Im cation, blue; anion, red; water molecule, purple). Left and right in (a) and (b) are the projection along the *a* axis and its stereoview, respectively, and those in (c) is the corresponding views.

moments of the two individual DD water molecules are pointing in opposite directions from each other. In $[\text{EMINN}]^+[\text{BANN}]^-$, however, the 2DD2AA structure was stabilized by binding with carboxylate anions and imidazolium cations (Figure 4a). These hydrogen bonds of water molecules produce the 1D tape structure of arylcarboxylate. In $[\text{EMINN}]_2^+[\text{BA}_2]^{2-}$, two water molecules with the 1D1A structure of D2¹⁶ which is typical of a discrete dimer, connect the one-side carboxylates in $[\text{BA}_2]^{2-}$ to form a 1D chain and eventually $[\text{EMINN}]_2^+[\text{BA}_2]^{2-}$ has a 2D sheet structure (Figure 4b). In $[\text{EMINN}]_3^+[\text{BA}_3]^{3-}$, a complicated network consisting of many water molecules (40 molecules in a unit cell) was observed (Figure 4c). The observed hydrogen bonds also produced a 2D sheet structure of arylcarboxylate.

There are no short contacts between the radical centers affecting the magnetic interaction within the tape and sheet structure. In the crystalline structure, the resulting tapes for $[\text{EMINN}]^+[\text{BANN}]^-$ were packed tightly to give a four-spin system, and the 2D sheets for $[\text{EMINN}]_2^+[\text{BA}_2]^{2-}$ and $[\text{EMINN}]_3^+[\text{BA}_3]^{3-}$ were layered to afford the 1D-spin networks due to the proximity of the NN spin centers, which are shown in Figure 5. In $[\text{EMINN}]^+[\text{BANN}]^-$, the NN centers of both cation and anion units within a tape were far ($>9 \text{ \AA}$) apart and the NN centers belonging to different tapes were close together. The shortest NO–NO distance ($\text{O}_2\text{--O}_2'$) is 4.10 \AA between

the cation units (the blue dashed lines in Figure 5a), while that ($\text{O}_1\text{--O}_3$) between the cation and the anion units is 4.24 \AA (the pink dashed lines in Figure 5a). Similarly, the crystal structure of $[\text{EMINN}]_2^+[\text{BA}_2]^{2-}$ and $[\text{EMINN}]_3^+[\text{BA}_3]^{3-}$ has the NO–NO short contacts to form a magnetic chain along the *b* axis. In $[\text{EMINN}]_2^+[\text{BA}_2]^{2-}$, the short NO–NO distances are repeated in the order of $3.28 (\text{O}_1\text{--O}_1')$ and $3.09 (\text{O}_2\text{--O}_2')$ \AA , and the resulting 1D chains align parallel to the *ab* plane (Figure 5b). In $[\text{EMINN}]_3^+[\text{BA}_3]^{3-}$, two chains A and B with short NO–NO distances repeating in the order of $3.14 (\text{O}_1\text{--O}_1')$ and $3.28 (\text{O}_2\text{--O}_3)$ \AA , and $3.23 (\text{O}_4\text{--O}_4')$, $3.15 (\text{O}_5\text{--O}_12)$, $3.22 (\text{O}_6\text{--O}_7)$, $3.20 (\text{O}_8\text{--O}_10)$, and $3.11 (\text{O}_9\text{--O}_11)$ \AA , respectively, exist in a 1:2 ratio and alternately align parallel as shown in Figure 5c. The direction of magnetic chains in $[\text{EMINN}]_2^+[\text{BA}_2]^{2-}$ and $[\text{EMINN}]_3^+[\text{BA}_3]^{3-}$ is shown in parts b and c, respectively, of Figure 4. In both salts, the shortest distance between the chains is $4.39 (\text{O}_1\text{--O}_1')$ for $[\text{EMINN}]_2^+[\text{BA}_2]^{2-}$ and $4.88 (\text{O}_3\text{--O}_11)$ \AA for $[\text{EMINN}]_3^+[\text{BA}_3]^{3-}$, indicating the interchain interactions to be weak.

The selected distances, dihedral angles, and short contacts between the NN centers for the four ion-pair molecules are summarized in Table 2.

In the molecular structure of each ion-pair molecule, a large dihedral angles (NN–Im = $51\text{--}58^\circ$) between the NN and imidazolium planes was observed, suggesting that the direct

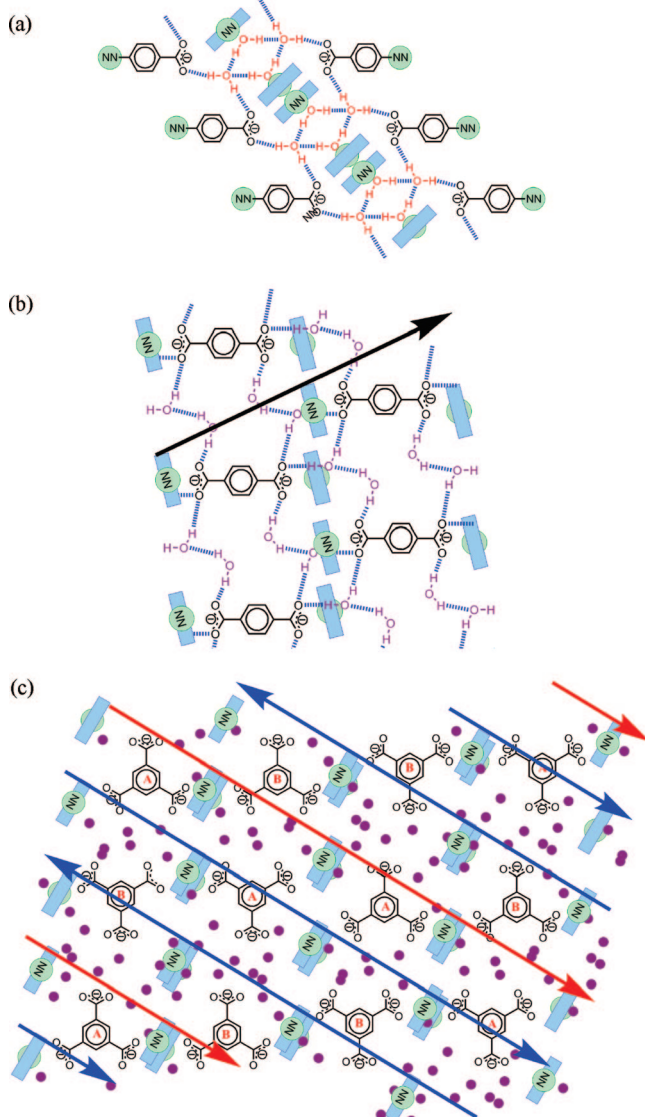


FIGURE 4. Schematic drawings of hydrogen bonds of water molecules among the carboxylates together with the $[\text{EMINN}]^+$ unit in (a) $[\text{EMINN}]^+[\text{BANN}]^-$, (b) $[\text{EMINN}]^+_2[\text{BA}_2]^{2-}$, and (c) $[\text{EMINN}]^+_3[\text{BA}_3]^{3-}$. The purple balls in (c) indicate water molecules. The arrows in (b) and red (chain A) and blue (chain B) arrows in (c) indicate the direction of the magnetic chain (see the text).

magnetic couplings between the NN centers are predominant and those through the imidazolium units can be ignored. In the magnetic couplings caused by the through-space interaction, not only the short distance between radical spin centers but also the relative geometry of NN centers is important.¹⁸ The shortest NO–NO distance ($r_{\text{NO–NO}}$) between the middle of the N–O bonds is 4.32 Å ($r_{\text{NO–NO}}$) for $[\text{EMINN}]^+[\text{Br}]^-$, 4.76 and 4.76 Å for the cation–cation and cation–anion pairs, respectively, in $[\text{EMINN}]^+[\text{BANN}]^-$, 3.18 and 3.48 Å for $[\text{EMINN}]^+_2[\text{BA}_2]^{2-}$, and 3.18–3.34 Å for $[\text{EMINN}]^+_3[\text{BA}_3]^{3-}$. The relative geometry of the nearest NN centers revealed by X-ray crystallography is shown in Figure 6, where the π orbitals containing the radical spin take an orthogonal position relative to the NN plane.

As shown in Figure 6a, the NN planes in $[\text{EMINN}]^+[\text{Br}]^-$ align parallel to each other and the overlap between the π orbital

(18) Akabane, R.; Tanaka, M.; Matsuo, K.; Koga, N.; Matsuda, K.; Iwamura, H. *J. Org. Chem.* **1997**, *62*, 8854–8861.

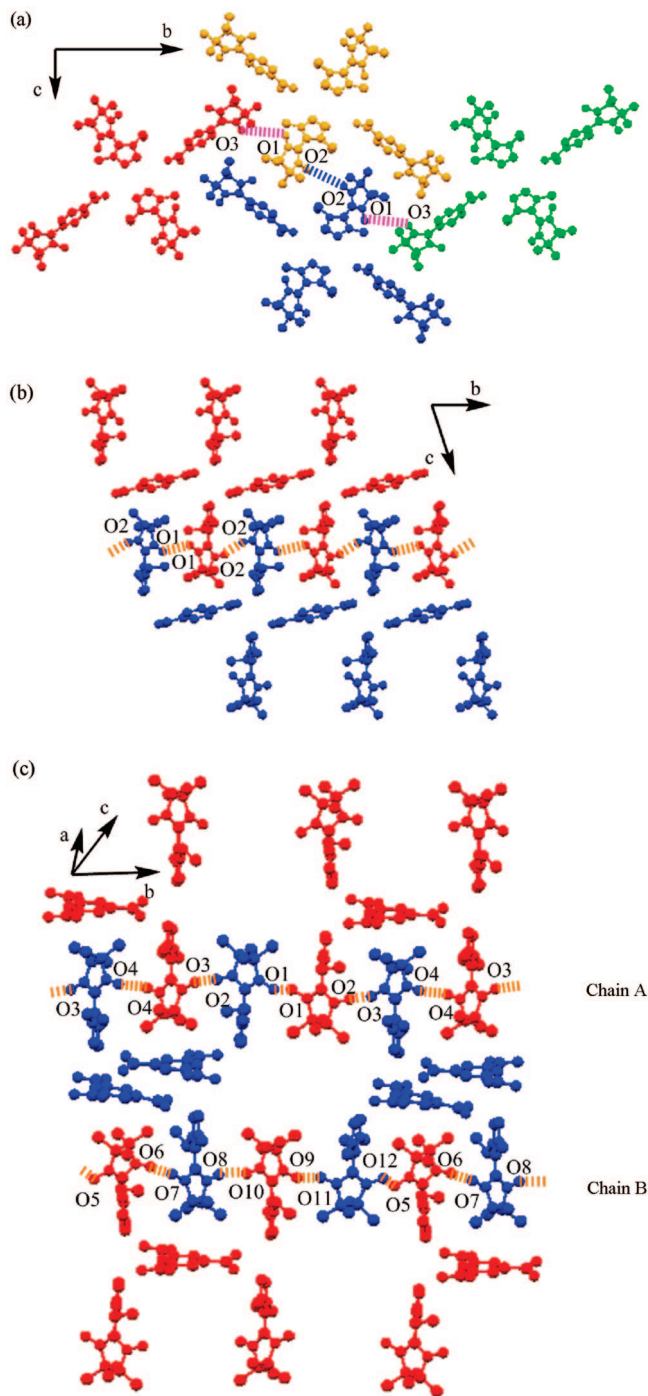


FIGURE 5. Crystal packings for (a) $[\text{EMINN}]^+[\text{BANN}]^-$, (b) $[\text{EMINN}]^+_2[\text{BA}_2]^{2-}$, and (c) $[\text{EMINN}]^+_3[\text{BA}_3]^{3-}$ with a ball-and-stick model. The same color shows the molecules in the same tape and plane, and the dashed lines indicate the NO–NO short contacts.

of the radical centers is unfavorable. Furthermore, taking the distance of 4.32 Å ($r_{\text{NO–NO}}$) into account, the magnetic interaction may be weak. In $[\text{EMINN}]^+[\text{BANN}]^-$, on the other hand, the overlap of the π orbital in the cation–cation pair is favorable, while the cation–anion pair is twisted and the overlap of the π orbital is unfavorable. The relative geometry indicates that in the magnetic coupling of $[\text{EMINN}]^+[\text{BANN}]^-$, the cation–cation pair predominates. However, the long distance of 4.76 Å ($r_{\text{NO–NO}}$) may give weak interaction. In both $[\text{EMINN}]^+_2[\text{BA}_2]^{2-}$ and $[\text{EMINN}]^+_3[\text{BA}_3]^{3-}$, the overlap of π

TABLE 2. Selected Dihedral Angles and Distances for [EMINN]⁺[BANN]⁻, [EMINN]₂[BA₂]²⁻, and [EMINN]₃[BA₃]³⁻^a

[EMINN] ⁺ [BANN] ⁻		[EMINN] ₂ [BA ₂] ²⁻		[EMINN] ₃ [BA ₃] ³⁻	
Dihedral Angles (deg) between the NN and Imidazolium Planes					
O1N1C1N2O2–C8C9C10	57.98	O1N1C1N2O2–C8C9C10	50.54	O1N1C1N2O2–C8C9C10	56.00
Anion (NN-phenyl ring)	29.01			O3N5C14N6O4–C21C22C23	54.14
O3N5C14N6O4–C21C23C25				O5N9C27N10O6–C34C35C36	54.96
				O7N13C40N14O8–C47C48C49	53.40
Shortest Distance between the Cation and the Anion					
C10–O6	3.04	C10–O4	3.49	O9N17C53N18O10–C60C61C62	50.59
Distances between the NN Centers (Å)					
cation–cation				O11N21C66N22O12–C73C74C75	51.31
O2–O2'	4.10 (4.76)	O1–O1'	3.28 (3.48)	O1–O1'	3.14 (3.27)
		O2–O2'	3.09 (3.18)	O2–O3	3.28 (3.34)
cation–anion				O4–O4'	3.23 (3.27)
O1–O3	4.24 (4.76)			O5–O12	3.15 (3.18)
				O6–O7	3.22 (3.25)
				O8–O10	3.20 (3.28)
				O9–O11	3.11 (3.29)

^a Numbers in parentheses are the distances between the middle of NO bonds.

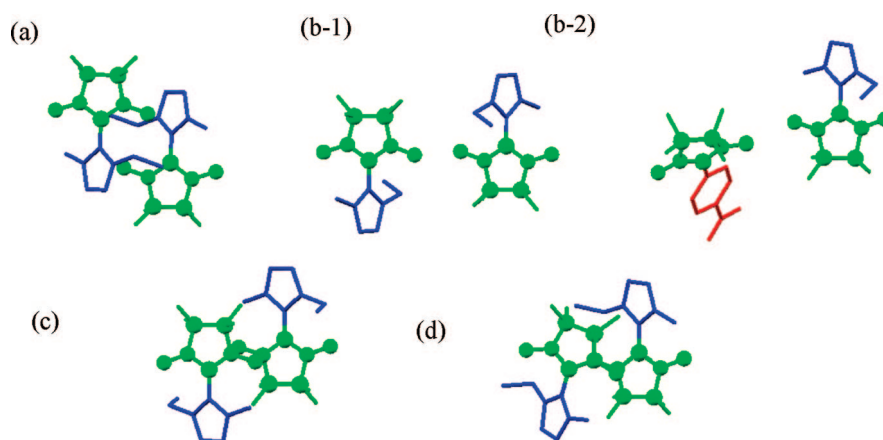


FIGURE 6. Relative geometry of the nearest NN centers in (a) [EMINN]⁺[Br]⁻, (b-1) cation–cation and (b-2) cation–anion pairs in [EMINN]⁺[BANN]⁻, (c) [EMINN]₂[BA₂]²⁻, and (d) [EMINN]₃[BA₃]³⁻ with a ball-and-stick model (color code: NN moiety, green; Im cation, blue; anion, red).

orbitals is favorable in addition to the short distance of 3.18–3.48 Å ($r_{\text{NO} \cdots \text{NO}}$), suggesting that strong antiferromagnetic interactions take place.

SQUID Measurements. The molar magnetic susceptibilities (χ_{mol}) of the microcrystalline samples of [EMINN]⁺[X]⁻ (X = Br, I, BPh₄, and TFSI), [EMINN]⁺[BANN]⁻, [EMINN]₂[BA₂]²⁻, and [EMINN]₃[BA₃]³⁻ were measured at a constant dc field of 5 kOe in the temperature range of 2–300 K.

The temperature dependence of χ_{mol} for [EMINN]⁺[Br]⁻ and [EMINN]⁺[BPh₄]⁻ is shown in Figure 7. The thermal profiles of [EMINN]⁺[I]⁻ and [EMINN]⁺[TFSI]⁻ were similar to that of [EMINN]⁺[Br]⁻ (Figure S3, Supporting Information). The values of $\chi_{\text{mol}}T$ at 300 K are 0.36 and 0.36 cm³ K mol⁻¹ for [EMINN]⁺[Br]⁻ and [EMINN]⁺[BPh₄]⁻, respectively, which are in good agreement with that (0.38) calculated by the spin only equation with $S = 1/2$. When the temperature decreased from 300 K, the $\chi_{\text{mol}}T$ values for [EMINN]⁺[Br]⁻ were nearly constant until 10 K and then slightly decreased below it, and those for [EMINN]⁺[BPh₄]⁻ were constant at all temperatures.

The thermal profiles observed in the $\chi_{\text{mol}}T$ vs T plots for [EMINN]⁺[Br]⁻ and [EMINN]⁺[BPh₄]⁻ are characteristic of isolated paramagnetic species. Notably, in [EMINN]⁺[BPh₄]⁻,

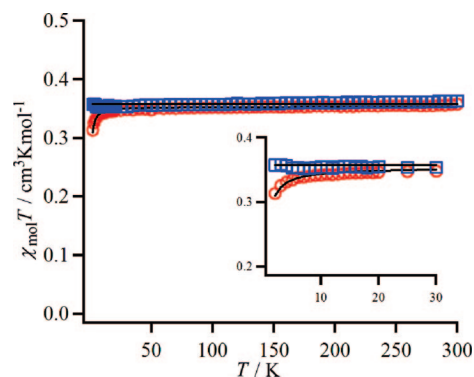


FIGURE 7. The $\chi_{\text{mol}}T$ vs T plots of [EMINN]⁺[Br]⁻ (○) and [EMINN]⁺[BPh₄]⁻ (□). The solid lines are fitting theoretical curves with the optimized parameters. See the text.

the spin center was completely isolated by the bulky anion, BPh₄. The values of $C = 0.35$ and 0.35 cm³ K mol⁻¹ and $\theta = -0.28$ and 0 K for [EMINN]⁺[Br]⁻ and [EMINN]⁺[BPh₄]⁻, respectively, were obtained using a Currie–Weiss equation; $\chi_{\text{mol}} = C/(T - \theta)$. The theoretical curves with these parameters for [EMINN]⁺[Br]⁻ and [EMINN]⁺[BPh₄]⁻ are shown in Figure

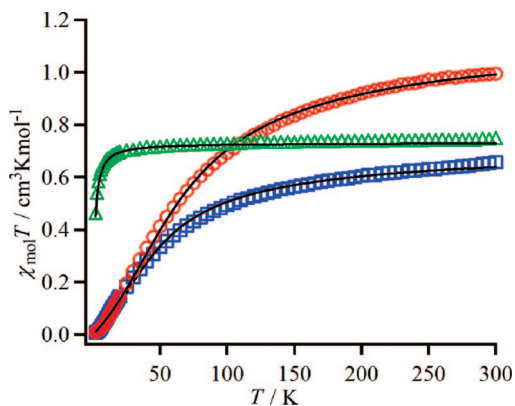


FIGURE 8. Plots of $\chi_{\text{mol}}T$ vs T for $[\text{EMINN}]^+[\text{BANN}]^-$ (Δ), $[\text{EMINN}]^+_2[\text{BA}_2]^{2-}$ (\square), and $[\text{EMINN}]^+_3[\text{BA}_3]^{3-}$ (\circ). The solid lines are theoretical curves with the optimized parameters.

7. $[\text{EMINN}]^+[\text{I}]^-$ also gave $C = 0.37 \text{ cm}^3 \text{ K mol}^{-1}$ and $\theta = -0.30 \text{ K}$ (Figure S3, Supporting Information). Taking the crystal packing revealed by X-ray crystallography into account, the data of $\chi_{\text{mol}}T$ vs T plot for $[\text{EMINN}]^+[\text{TFSI}]^-$ were analyzed by a Bleaney–Bowers equation.¹⁹ The value of $g = 2.0076$ obtained from ESR spectra for the crystalline sample was used, and the best fitting parameters, $J/k_B = -2.2 \text{ K}$ and $w = 0.98$, were obtained (Figure S3, Supporting Information).

The temperature dependence of χ_{mol} for $[\text{EMINN}]^+[\text{BANN}]^-$, $[\text{EMINN}]^+_2[\text{BA}_2]^{2-}$, and $[\text{EMINN}]^+_3[\text{BA}_3]^{3-}$, is summarized in Figure 8. The $\chi_{\text{mol}}T$ values at 300 K are 0.74, 0.66, and 1.00 $\text{cm}^3 \text{ K mol}^{-1}$ for $[\text{EMINN}]^+[\text{BANN}]^-$, $[\text{EMINN}]^+_2[\text{BA}_2]^{2-}$, and $[\text{EMINN}]^+_3[\text{BA}_3]^{3-}$, respectively. The value for $[\text{EMINN}]^+[\text{BANN}]^-$ is consistent with that (0.75) calculated using a spin-only equation with isolated two and three spins, while the values for $[\text{EMINN}]^+_2[\text{BA}_2]^{2-}$ and $[\text{EMINN}]^+_3[\text{BA}_3]^{3-}$ are slightly smaller (0.75 and 1.13). When the temperature decreased from 300 K, the $\chi_{\text{mol}}T$ values for $[\text{EMINN}]^+[\text{BANN}]^-$ were nearly constant until 20 K and then decreased. On the other hand, those for $[\text{EMINN}]^+_2[\text{BA}_2]^{2-}$ and $[\text{EMINN}]^+_3[\text{BA}_3]^{3-}$ gradually decreased and reached zero at 2 K. The small values at 300 K and thermal profiles of the $\chi_{\text{mol}}T$ values $[\text{EMINN}]^+_2[\text{BA}_2]^{2-}$ and $[\text{EMINN}]^+_3[\text{BA}_3]^{3-}$ indicate that strong antiferromagnetic interaction operates even at 300 K.

In order to understand the magnetic properties quantitatively, a four-spin model,²⁰ $H = -2J_1(S_1S_2 + S_3S_4) - 2J_2S_2S_3$, for $[\text{EMINN}]^+[\text{BANN}]^-$ and an antiferromagnetic chain model,²¹ $H = -J\sum S_iS_{i+1}$, for $[\text{EMINN}]^+_2[\text{BA}_2]^{2-}$ and $[\text{EMINN}]^+_3[\text{BA}_3]^{3-}$ suggested by X-ray crystal structure analysis were applied to the spin systems. In $[\text{EMINN}]^+_2[\text{BA}_2]^{2-}$ and $[\text{EMINN}]^+_3[\text{BA}_3]^{3-}$, although the distances between NN centers revealed by X-ray crystallography are different, it is assumed that they are equal. The experimental data for $[\text{EMINN}]^+[\text{BANN}]^-$ and for $[\text{EMINN}]^+_2[\text{BA}_2]^{2-}$ and $[\text{EMINN}]^+_3[\text{BA}_3]^{3-}$ were fitted by the theoretical equation, in which a mass factor, w , and $g = 2.0076$ obtained from the ESR spectra of

(19) Bleaney, B.; Bowers, K. D. *Proc. R. Soc. London Ser. A* **1952**, *214*, 451–465.

(20) Rubenacker, G. V.; Drumheller, J. E.; Emerson, K.; Willet, R. D. *J. Magn. Magn. Mater.* **1986**, *54*, 1483–1484.

(21) Estes, W. E.; Gavel, D. P.; Hatfield, W. E.; Hodgson, D. J. *Inorg. Chem.* **1978**, *17*, 1415–1421.

(22) (a) Nagashima, H.; Inoue, H.; Yoshioka, N. *J. Phys. Chem. B* **2004**, *108*, 6144–6151. (b) Pal, S. K.; Itkis, M. E.; Reed, R. W.; Oakley, R. T.; Cordes, A. W.; Tham, F. S.; Siegrist, T.; Haddon, R. C. *J. Am. Chem. Soc.* **2004**, *126*, 1478–1484. (c) Hicks, R. G.; Lemaire, M. T.; Ohlstrom, L.; Richardson, J. F.; Thompson, L. K.; Xu, Z. *J. Am. Chem. Soc.* **2001**, *123*, 7154–7159.

TABLE 3. Detected Signals in ESI-Mass Spectra for $[\text{EMINN}]^+[\text{Br}]^-$, $[\text{EMINN}]^+[\text{BA}]^-$, $[\text{EMINN}]^+[\text{BANN}]^-$, $[\text{EMINN}]^+_2[\text{BA}_2]^{2-}$, and $[\text{EMINN}]^+_3[\text{BA}_3]^{3-}$

$[\text{EMINN}]^+[\text{Br}]^-$	266.22 ($[\text{EMINN}]^+$), 611.38 ($[\text{EMINN}]^+ + [\text{EMINN}]^+[\text{Br}]^-$), 958.54 ($[\text{EMINN}]^+ + ([\text{EMINN}]^+[\text{Br}]^-)_2$)
$[\text{EMINN}]^+[\text{BA}]^-$	266.28 ($[\text{EMINN}]^+$), 653.58 ($[\text{EMINN}]^+ + [\text{EMINN}]^+[\text{BA}]^-$), 1040.92 ($[\text{EMINN}]^+ + ([\text{EMINN}]^+[\text{BA}]^-)_2$)
$[\text{EMINN}]^+[\text{BANN}]^-$	266.15 ($[\text{EMINN}]^+$), 808.4 ($[\text{EMINN}]^+ + [\text{EMINN}]^+[\text{BANN}]^-$), 1894.05 ($([\text{EMINN}]^+ + ([\text{EMINN}]^+[\text{BANN}]^-)_2$)
$[\text{EMINN}]^+_2[\text{BA}_2]^{2-}$	266.16 ($[\text{EMINN}]^+$), 962.55 ($[\text{EMINN}]^+ + [\text{EMINN}]^+_2[\text{BA}_2]^{2-}$), 1660.00 ($[\text{EMINN}]^+ + ([\text{EMINN}]^+_2[\text{BA}_2]^{2-})_2$)
$[\text{EMINN}]^+_3[\text{BA}_3]^{3-}$	266.16 ($[\text{EMINN}]^+$), 1006.53 ($[\text{EMINN}]^+_3[\text{BA}_3]^{3-} + 1$), 1271.74 ($[\text{EMINN}]^+ + [\text{EMINN}]^+_3[\text{BA}_3]^{3-}$)

powdered samples were used. The best-fitting parameters are the spin-exchange coupling parameters, $J_1/k_B = -0.27$, $J_2/k_B = -0.16 \text{ K}$ and $w = 0.97$ for $[\text{EMINN}]^+[\text{BANN}]^-$ and $J/k_B = -62.1$ and -86.5 K and $w = 0.96$ and 1.04 for $[\text{EMINN}]^+_2[\text{BA}_2]^{2-}$ and $[\text{EMINN}]^+_3[\text{BA}_3]^{3-}$, respectively. The best-fit curves are shown in Figure 8 as solid curves. The J_1/k_B and J_2/k_B values for $[\text{EMINN}]^+[\text{BANN}]^-$ were very small, indicating that the magnetic couplings were weak and nearly insignificant, as anticipated from the crystal packing. The large negative values for $[\text{EMINN}]^+_2[\text{BA}_2]^{2-}$ and $[\text{EMINN}]^+_3[\text{BA}_3]^{3-}$ were due to the through-space antiferromagnetic interaction and are often obtained in tightly packed crystals of organic radicals.²²

ESI-Mass Spectra, ESR Spectra, and Relaxivity Measurements in Solution. (A) ESI-Mass Spectral Measurements. In order to confirm the association of cation–anion ion pairs in solution, ESI-mass spectra (Figure S4, Supporting Information) were measured in the positively charged mode. The solutions (50 μM) of $[\text{EMINN}]^+[\text{Br}]^-$, $[\text{EMINN}]^+[\text{BA}]^-$, $[\text{EMINN}]^+[\text{BANN}]^-$, $[\text{EMINN}]^+_2[\text{BA}_2]^{2-}$, and $[\text{EMINN}]^+_3[\text{BA}_3]^{3-}$ in acetonitrile were used as the samples. The parent ion-pair molecule, $[\text{EMINN}]^+[\text{Br}]^-$, showed signals at 611.38 and 958.54 due to the ion pair clusters, $[\text{EMINN}]^+ + ([\text{EMINN}]^+[\text{Br}]^-)_n$; $n = 1$ and 2, in addition to one at 266.22 for the free imidazolium cation, $[\text{EMINN}]^+$. Similarly, other salts showed signals for the monomer cluster (the free imidazolium cation + the corresponding cation–anion salts) and the dimer cluster as summarized in Table 3. Only in the spectrum for $[\text{EMINN}]^+_3[\text{BA}_3]^{3-}$ was the signal due to $[\text{EMINN}]^+_3[\text{BA}_3]^{3-} + 1$ observed, while the one for the dimer cluster was not. The lack of a signal for the higher cluster might suggest that the cation unit loosely binds to the anion by the conjunction caused by the increase in the number of relatively bulky cation units. Observed positive-ion mass spectra were typical for IL salts, which were reported in the literature.²³ These results suggested that the cation units in $[\text{EMINN}]^+[\text{BANN}]^-$, $[\text{EMINN}]^+_2[\text{BA}_2]^{2-}$, and $[\text{EMINN}]^+_3[\text{BA}_3]^{3-}$ are bound with an anion unit to form the 1:1, 2:1, and 3:1 cation–anion salts, respectively, even in solution.

(B) ESR Spectral Measurements. The ESR spectra at 25 $^\circ\text{C}$ for the samples in solution ($\sim 1 \text{ mM}$) of $[\text{EMINN}]^+[\text{Br}]^-$ in H_2O and EtOH showed typical five-line signals (signal intensity; 1:2:3: 2:1) due to the NN moieties with $g = 2.0072$ and 2.0070 and hyperfine coupling constant, $a_N = 7.51$ and 7.08 gauss,

(23) (a) Bini, R.; Bortolini, O.; Chiappe, C.; Pieraccini, D.; Siciliano, T. *J. Phys. Chem. B* **2007**, *111*, 598–604. (b) Nobuoka, K.; Kitaoka, S.; Kunimitsu, K.; Iio, M.; Harran, T.; Wakisaka, A.; Ishikawa, Y. *J. Org. Chem.* **2005**, *70*, 10106–10108. (c) Gozzo, F. C.; Santos, L. S.; Augusti, R.; Consorti, C. S.; Dupont, J.; Eberlin, M. N. *Chem.—Eur. J.* **2004**, *10*, 6187–6193.

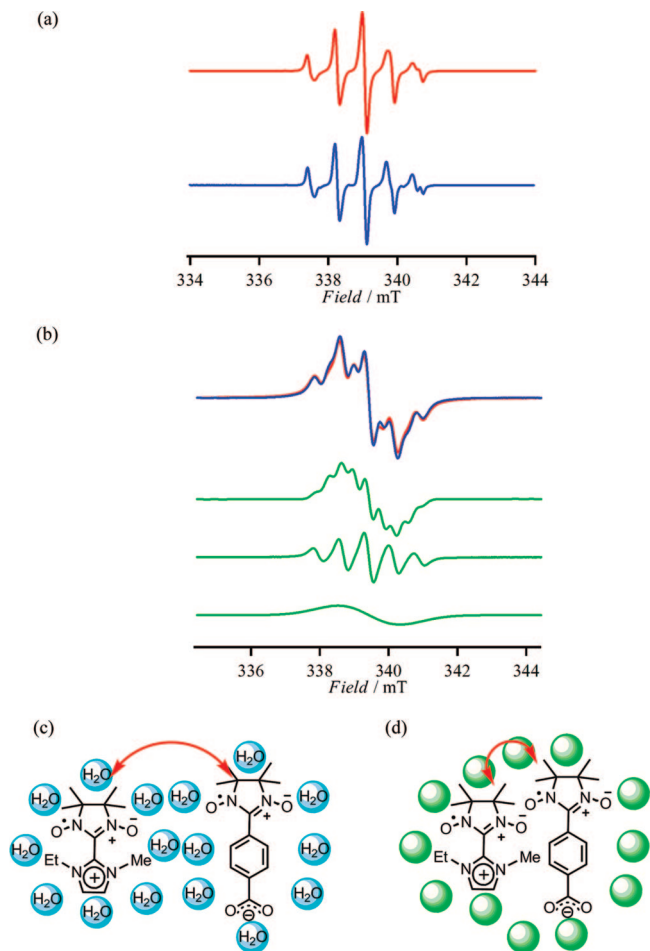


FIGURE 9. ESR spectra of $[\text{EMINN}]^+[\text{BANN}]^-$ in (a) water and (b) 2% EtOH in toluene at 25 °C. In (a), the upper and lower spectrum are experimental and the summation of ones for $[\text{EMINN}]^+$ and $[\text{BANN}]^-$ units, respectively. In (b), the red- and blue-line spectra are the ones for the experimental and the summation of the (i) nine-line spectrum, (ii) five-line spectrum, and (iii) one-line spectrum, respectively. Schematic drawing of the role of solvent molecules in (c) H_2O and (d) 2% EtOH in toluene.

respectively. The increase in the value of a_N , of NN in water can be explained by the hydrogen bonding between the hydrogen of the water molecule and the oxygen of NN.²⁴

The ESR spectra for $[\text{EMINN}]^+[\text{BANN}]^-$ strongly depended on the solvent (Figure 9). The spectrum in H_2O and EtOH showed typical five-line signals (Figure 9a), while that in toluene containing 2% EtOH showed a mixture of nine-line, five-line, and broad one-line signals (Figure 9b). The former spectrum in H_2O was represented by the summation of two five-line signals with $g = 2.0072$ and 2.0071 , and $a_N/2 = 7.5$ and 8.1 gauss for $[\text{EMINN}]^+$ and $[\text{BANN}]^-$ units, respectively, indicating that in protic solvents such as H_2O and EtOH a cation–anion pair might be dissociated by solvent molecules and showed no magnetic interactions (Figure 9c). The latter spectrum was represented as the summation of the nine-line signal (diradical simulation, $g = 2.0076$, $a_N/2 = 7.2$ and 6.8 gauss, $|2J/g\mu_B| = 50$ gauss, line width = 3.3 gauss), the five-line signal ($g = 2.0076$ and $a_N/2 = 7.52$ gauss), and broad one-line signal ($g = 2.0076$, line width = 18 gauss) in a ratio of 50:19:31. The nine-line and one-line broad signals are due to the species in which

TABLE 4. Values of r_1 and r_2 for $[\text{EMINN}]^+[\text{Br}]^-$, $[\text{EMINN}]^+[\text{BA}]^-$, $[\text{EMINN}]^+[\text{BANN}]^-$, $[\text{EMINN}]^+_2[\text{BA}_2]^{2-}$, and $[\text{EMINN}]^+_3[\text{BA}_3]^{3-}$, at 25 MHz and 25 °C^a

	r_1 , $\text{mM}^{-1} \text{s}^{-1}$	r_2 , $\text{mM}^{-1} \text{s}^{-1}$
$[\text{EMINN}]^+[\text{Br}]^-$	0.13	0.17
$[\text{EMINN}]^+[\text{BA}]^-$	0.14	0.13
$[\text{EMINN}]^+[\text{BANN}]^-$	0.32 (0.16)	0.31 (0.16)
$[\text{EMINN}]^+_2[\text{BA}_2]^{2-}$	0.26 (0.13)	0.30 (0.15)
$[\text{EMINN}]^+_3[\text{BA}_3]^{3-}$	0.40 (0.13)	0.46 (0.15)

^a The values in parentheses are relaxivity per radical.

two NN spins interact weakly and strongly, respectively, and the five-line signal is due to the magnetically isolated NN spin. The line broadening is might be due to incomplete averaging of anisotropy, most likely D value. The existence of the nine-line and one-line broad signals in the simulation experiment²⁵ suggested that the distance of the radical centers between the cation and the anion units was shortened by the surrounding solvent molecules, as shown in Figure 9d.

These ESR spectra for $[\text{EMINN}]^+_2[\text{BA}_2]^{2-}$ and $[\text{EMINN}]^+_3[\text{BA}_3]^{3-}$ at 25 °C in H_2O showed the five-line signals without any line broadening similar to that for $[\text{EMINN}]^+[\text{BANN}]^-$. No observations of significant line broadening indicate that the NN spin centers are separated by the surrounding water molecules and are magnetically isolated in H_2O .

(C) Relaxivity Measurements. The spin–lattice and the spin–spin relaxation rate ($1/T_1$ and $1/T_2$, respectively) of the solution samples (ca. 1, 2, and 5 mM) were measured at 25 °C by a pulse NMR spectrometer (25 MHz, 0.59 T) (Figure S5, Supporting Information). The relaxivity values r_1 and r_2 were obtained from the concentration dependence of T_1 and T_2 (see the Experimental Section). The values of relaxivity for monoradicals, $[\text{EMINN}]^+[\text{Br}]^-$ and $[\text{EMINN}]^+[\text{BA}]^-$, were 0.13 and 0.14 for r_1 and 0.17 and 0.13 $\text{mM}^{-1} \text{s}^{-1}$ for r_2 , respectively, which were consistent with that reported previously.²⁶ In $[\text{EMINN}]^+_2[\text{BA}_2]^{2-}$, and $[\text{EMINN}]^+_3[\text{BA}_3]^{3-}$, the r_1 per molecule was 0.26 and 0.40 $\text{mM}^{-1} \text{s}^{-1}$, respectively, and increased along with the number of $[\text{EMINN}]^+$ units. Those values per radical correspond to that for $[\text{EMINN}]^+[\text{BA}]^-$, indicating that the translational correlation time²⁷ is dominant in this spin system. For $[\text{EMINN}]^+[\text{BANN}]^-$, the r_1 value of 0.32 $\text{mM}^{-1} \text{s}^{-1}$ is slightly larger than the one (0.26) for $[\text{EMINN}]^+_2[\text{BA}_2]^{2-}$ due to the NN belonging to $[\text{BANN}]^-$ whose r_1 value is 0.19 $\text{mM}^{-1} \text{s}^{-1}$. In this series of cation–anion pair molecules prepared by simple ion-exchange reaction, the relaxivity was confirmed to increase with the increase in the number of radical units. The values of r_1 and r_2 for $[\text{EMINN}]^+[\text{Br}]^-$, $[\text{EMINN}]^+[\text{BA}]^-$, $[\text{EMINN}]^+[\text{BANN}]^-$, $[\text{EMINN}]^+_2[\text{BA}_2]^{2-}$, and $[\text{EMINN}]^+_3[\text{BA}_3]^{3-}$ are listed in Table 4.

Conclusion

A water-soluble radical salt, $[\text{EMINN}]^+[\text{Br}]^-$, was prepared as a parent molecule. Its anion unit in $[\text{EMINN}]^+[\text{Br}]^-$ was exchanged by the anion-exchange reaction with arylcarboxylic acid to form the 1:1 ion-pair molecules, $[\text{EMINN}]^+[\text{BANN}]^-$ and $[\text{EMINN}]^+[\text{BA}]^-$, and the 1:2, and 1:3 ion-pair molecules, $[\text{EMINN}]^+_2[\text{BA}_2]^{2-}$ and $[\text{EMINN}]^+_3[\text{BA}_3]^{3-}$, respectively. Those

(25) Kirste, B. BIRADG program. *Anal. Chim. Acta* **1992**, *265*, 191–200.

(26) (a) Spagnol, G.; Shiraishi, K.; Rajca, S.; Rajca, A. *Chem. Commun.* **2005**, 5047–5049. (b) Francesc, G.; Dunand, F. A.; Loosli, C.; Merbach, A. E.; Decurtins, S. *Magn. Reson. Chem.* **2003**, *41*, 81–83.

(27) Polnaszek, C. F.; Bryant, R. G. *J. Chem. Phys.* **1984**, *81*, 4038–4045.

(24) Griffith, O. H.; Dehlinge, P. J.; Van, S. P. *J. Membr. Biol.* **1974**, *15*, 159–192.

molecular and crystal structures were characterized by X-ray crystallography and the magnetic properties of those crystal samples were investigated. In the crystal structure, the molecules of $[\text{EMINN}]^+[\text{X}]^-$ formed a dimer structure of the cation–anion pair, in which the anion units were located near C9 and C10 in the imidazolium cation, while arylcarboxylate salts showed a tape structure for $[\text{EMINN}]^+[\text{BANN}]^-$ and a sheet structure for $[\text{EMINN}]_2^+[\text{BA}_2]^{2-}$ and $[\text{EMINN}]_3^+[\text{BA}_3]^{3-}$ via hydrogen bonds with the water molecules. The resulting tape and sheets were layered to afford a magnetically linear four–spin structure consisting of the NO–NO short contacts of the cation–cation and cation–anion units for $[\text{EMINN}]^+[\text{BANN}]^-$ and linear chain structures of those of the cation units for $[\text{EMINN}]_2^+[\text{BA}_2]^{2-}$ and $[\text{EMINN}]_3^+[\text{BA}_3]^{3-}$. The experimental data of $\chi_{\text{mol}}T$ vs T plots for $[\text{EMINN}]^+[\text{BANN}]^-$, $[\text{EMINN}]_2^+[\text{BA}_2]^{2-}$, and $[\text{EMINN}]_3^+[\text{BA}_3]^{3-}$, were fitted by theoretical equations to give the exchange coupling parameters, $J_1/k_B = -0.27$ and $J_2/k_B = -0.16$ K by a four-spin model for $[\text{EMINN}]^+[\text{BANN}]^-$, and $J/k_B = -62.1$, and -86.5 K by an antiferromagnetic linear-chain model for $[\text{EMINN}]_2^+[\text{BA}_2]^{2-}$ and $[\text{EMINN}]_3^+[\text{BA}_3]^{3-}$, respectively.

In solution, on the other hand, the magnetic properties of salts strongly depend on the solvent. In water or an EtOH solution, the ESR spectra of all salts showed no significant interaction between the radical centers, while in 2% EtOH in toluene, $[\text{EMINN}]^+[\text{BANN}]^-$ showed a spectrum containing a nine-line signal at room temperature. Taking the detection of the peak of a parent salt plus a free imidazolium cation by ESI mass spectrometry into account, the lack of magnetic interaction in the protic solvents (water and EtOH) may suggest that the solvent molecules separate the cation and anion units by the hydrogen bond, especially with the anion units and lengthen the distance between the radical centers in the cation units within a molecule. That the cation–anion interaction is weak in the protic solvents, was evident from the relaxivity values. The water-proton relaxivity of the salts is $r_1 = 0.13, 0.14, 0.32, 0.26,$ and 0.40 and $r_2 = 0.17, 0.13, 0.31, 0.30,$ and 0.46 $\text{mM}^{-1} \text{sec}^{-1}$ for $[\text{EMINN}]^+[\text{Br}]^-$, $[\text{EMINN}]^+[\text{BA}]^-$, $[\text{EMINN}]^+[\text{BANN}]^-$, $[\text{EMINN}]_2^+[\text{BA}_2]^{2-}$, and $[\text{EMINN}]_3^+[\text{BA}_3]^{3-}$, respectively, and increased in proportion to the number of $[\text{EMINN}]^+$ units.

In this study, the assembly of organic spins by the ion-exchange reaction was confirmed with small molecules. When $[\text{EMINN}]^+$ was applied to a poly(carboxylate) molecule of large size, a molecule with high water-proton relaxivity values might be expected to form. However, the increase in relaxivity caused by large molecular size can not be expected, because the cation and anion units bound loosely to each other and thus the local rotational correlation time might be dominant. Along this line, attempts to obtain high relaxivity per molecule are in progress.

Experimental Section

X-ray Crystal and Molecular Structure Analyses. Crystallographic data and experimental details are summarized in Table S1 (Supporting Information) for $[\text{EMINN}]^+[\text{X}]^-$ ($\text{X} = \text{Br}, \text{I}, \text{TFSI},$ and BPh_4) and in Table S2 (Supporting Information) for $[\text{EMINN}]^+[\text{BANN}]^-$, $[\text{EMINN}]_2^+[\text{BA}_2]^{2-}$, and $[\text{EMINN}]_3^+[\text{BA}_3]^{3-}$. Suitable single crystals were glued onto a glass fiber using grease. All X-ray data were collected on a diffractometer with graphite-

monochromated Mo K α radiation ($\lambda = 0.71069$ Å). Reflections were collected at 123–138 K. The molecular structures were solved by direct methods (SIR program)²⁸ and expanded using Fourier techniques (DIRDIF99).²⁹ The refinements were converged using the full-matrix least-squares method from the Crystal Structure software package³⁰ to give $P2_1/c$ (no. 14) for $[\text{EMINN}]^+[\text{Br}]^-$, $[\text{EMINN}]^+[\text{BPh}_4]^-$, and $[\text{EMINN}]^+[\text{BANN}]^-$, $P2_1/n$ (no. 14) for $[\text{EMINN}]^+[\text{I}]^-$, and $P-1$ (no. 2) for $[\text{EMINN}]^+[\text{TFSI}]^-$, $[\text{EMINN}]_2^+[\text{BA}_2]^{2-}$, and $[\text{EMINN}]_3^+[\text{BA}_3]^{3-}$. All non-hydrogen atoms were refined anisotropically; hydrogen atoms in $[\text{EMINN}]^+[\text{I}]^-$, $[\text{EMINN}]^+[\text{BANN}]^-$, and $[\text{EMINN}]_3^+[\text{BA}_3]^{3-}$ were included at standard positions ($\text{C}-\text{H} = 0.96$ Å, $\text{C}-\text{C}-\text{H} = 120^\circ$) and refined isotropically using a rigid model, and those in the other salts were refined isotropically. Crystallographic data for the structure reported in this paper have been deposited with the Cambridge Crystallographic Data Center as supplementary publication no. CCDC-670821, 678889, 678890, 678891, 670823, 670822, and 672372 for $[\text{EMINN}]^+[\text{X}]^-$, $\text{X} = \text{Br}, \text{I}, \text{TFSI},$ and BPh_4 , $[\text{EMINN}]^+[\text{BANN}]^-$, $[\text{EMINN}]_2^+[\text{BA}_2]^{2-}$, and $[\text{EMINN}]_3^+[\text{BA}_3]^{3-}$, respectively.

ESR Spectra. ESR spectra were recorded on an X-band (9.4 GHz) spectrometer equipped with a microwave frequency counter. Sample solutions in H₂O were placed in capillary tubes and were measured at 25 °C.

Relaxivity Measurements. The spin–lattice and spin–spin relaxation rates (T_1 and T_2 , longitudinal and transverse relaxation time, respectively) were obtained on a spectrometer (25 MHz, 0.59 T). The sample solutions (ca. 1, 2, and 5 mM) in H₂O were placed in 10 mm o.d. glass tubes and were measured at 25 °C. The values of relaxivities, r_1 and r_2 , were calculated with equations (1) and (2).

$$1/T_1 = 1/T_0 + r_1C \quad (1)$$

$$1/T_2 = 1/T_0 + r_2C \quad (2)$$

where T_0 and C are the relaxation rate in the absence of the paramagnetic species and the concentration of the paramagnetic species, respectively.

Magnetic Susceptibility Measurements. Direct current (dc) magnetic susceptibility data were obtained on SQUID magneto/susceptometer and corrected for the magnetization of the sample holder and capsule and for diamagnetic contributions to the samples, which were estimated from Pascal's constants.^{3a}

Materials. 2,3-Bis(hydroxyamino)-2,3-dimethylbutane sulfate monohydrate,³¹ 1-methyl-2-formylimidazole,³² and 4-(1-oxy-3-oxo-4,4,5,5-tetramethylimidazolin-2-yl)benzoic acid (BANN)³³ were prepared by the procedure reported in the literature. Lithium salts, $\text{Li}^+[\text{TFSI}]^-$, $\text{Na}^+[\text{BPh}_4]^-$, and arylcarboxylic acid were purchased and used without purification.

1-Methyl-2-(1,3-oxo-4,4,5,5-tetramethylimidazolin-2-yl)imidazole, MINN(OH). 2,3-Bis(hydroxyamino)-2,3-dimethylbutane sulfate monohydrate (16.4 g, 62.1 mmol) was added to a solution of 1-methyl-2-formylimidazole (3.0 g, 27.2 mmol) in H₂O (70 mL), and the solution was stirred for 1 h. After neutralization with sodium carbonate, the reaction mixture was stirred for 1 h and the solvent was removed to dryness under reduced pressure. The crude mixture obtained was chromatographed on silica gel with $\text{CHCl}_3/\text{MeOH}$ (50/1) as the eluent to afford MINN(OH) as a white solid in 71.4%

(29) DIRDIF99: Beurskens, P. T.; Admiraal, G.; Beurskens, G.; Bosman, W. P.; de Gelder, R.; Israel, R.; Smits, J. M. M. The DIRDIF-99 program system, Technical Report of the Crystallography Laboratory, University of Nijmegen, The Netherlands, 1999.

(30) Crystal Structure 3.8: *Crystal Structure Analysis Package, Rigaku and Rigaku/MS* (2000–2006); 9009 New Trails Dr., The Woodlands, TX 77381.

(31) Ovcharenko, V.; Fokin, S.; Rey, P. *Mol. Cryst. Liq. Cryst.* **1999**, *334*, 109–119.

(32) LaRonde, F. J.; Brook, M. A. *Inorg. Chim. Acta* **1999**, *296*, 208–221.

(33) Inoue, K.; Iwamura, H. *Chem. Phys. Lett.* **1993**, *207*, 551–554.

(28) (a) Altomare, A.; Cascarano, G.; Giacovazzo, C.; Guagliardi, A.; Burla, M. C.; Polidori, G.; Camalli, M. *SIR92. J. Appl. Crystallogr.* **1994**, *27*, 435. (b) Altomare, A.; Burla, M. C.; Camalli, M.; Cascarano, G. L.; Giacovazzo, C.; Guagliardi, A.; Moliterni, A. G. G.; Polidori, G.; Spagna, R. *SIR97. J. Appl. Crystallogr.* **1999**, *32*, 115–119.

yield (4.67 g, 19.4 mmol): mp 176 – 177 °C dec; IR (KBr) 3252 cm^{-1} ; $^1\text{H NMR}$ (CDCl_3 , 270 MHz) δ 7.06 (s, 1H), 6.85 (s, 1H), 5.14 (s, 1H), 3.76 (s, 3H), 1.22 (s, 6H), 1.21 (s, 6H); mass spectrum (FAB, *m*-nitrobenzyl alcohol matrix) m/z 241.2 [$\text{M} + 1$]. Anal. Calcd for $\text{C}_{11}\text{H}_{20}\text{N}_4\text{O}_2$: C, 54.98; H, 8.39; N, 23.32. Found: C, 54.85; H, 8.31; N, 23.21.

1-Methyl-2-(1-oxy-3-oxo-4,4,5,5-tetramethylimidazolin-2-yl)imidazole, MINN. Lead oxide (10.5 g, 43.9 mmol) was added to a solution of MINN(OH) (1.78 g, 7.41 mmol) in CH_2Cl_2 (120 mL), and the suspension was stirred for 1 h at room temperature. After the filtration, the solvent was removed on a rotary evaporator. The crude mixture was chromatographed on silica gel with CHCl_3 as the eluent to give MINN as a blue solid in 84.7% yield (1.49 g 6.28 mmol): mp 155 – 157 °C; mass spectrum (FAB, *m*-nitrobenzyl alcohol matrix) m/z 238.2 [$\text{M} + 1$] $^+$, ESR (H_2O), $g = 2.0071$, $a_{\text{N}}/2 = 7.83$ gauss. Anal. Calcd for $\text{C}_{11}\text{H}_{20}\text{N}_4\text{O}_2$: C, 55.68; H, 7.22; N, 23.61. Found: C, 55.63; H, 7.25; N, 23.52.

1-Ethyl-2-(1-oxy-3-oxo-4,4,5,5-tetramethylimidazolin-2-yl)-3-methylimidazolium Bromide, [EMINN] $^+$ [Br] $^-$. Bromoethane (15 mL, 201 mmol) was added to a solution of MINN (650 mg, 2.74 mmol) in toluene (15 mL). The solution was refluxed for 3 days. The resulting precipitates were collected by filtration. The crude mixture was recrystallized from CH_2Cl_2 -Et $_2\text{O}$ to give [EMINN] $^+$ [Br] $^-$ as blue blocks in 88.8% yield (842 mg, 2.43 mmol): mp 208–210 °C dec; IR (KBr) 1379 cm^{-1} ; mass spectrum (FAB, *m*-nitrobenzyl alcohol matrix) m/z 266.4 [EMINN] $^+$, ESR (H_2O) $g = 2.0072$, $a_{\text{N}}/2 = 7.51$ gauss. Anal. Calcd for $\text{C}_{13}\text{H}_{22}\text{N}_4\text{O}_2$: C, 45.10; H, 6.40; N, 16.18. Found: C, 45.27; H, 6.39; N, 16.33.

1-Ethyl-2-(1-oxy-3-oxo-4,4,5,5-tetramethylimidazolin-2-yl)-3-methylimidazolium Iodide, [EMINN] $^+$ [I] $^-$. Iodoethane (1 mL, 304 mmol) was added to a solution of MINN (150 mg, 0.63 mmol) in chloroform (1 mL). The solution was refluxed for 5 h. After the addition of diethyl ether, the resulting precipitates were collected by filtration. The crude mixture was recrystallized from CH_2Cl_2 -Et $_2\text{O}$ to give [EMINN] $^+$ [I] $^-$ as blue blocks in 74.4% yield (185 mg, 0.47 mmol): mp 175 °C dec; IR (KBr) 1378 cm^{-1} ; mass spectrum (FAB, *m*-nitrobenzyl alcohol matrix) m/z 266.3 [EMINN] $^+$, ESR (H_2O) $g = 2.0073$, $a_{\text{N}}/2 = 7.50$ gauss. Anal. Calcd for $\text{C}_{13}\text{H}_{22}\text{N}_4\text{O}_2\text{I}$: C, 39.71; H, 5.64; N, 14.25. Found: C, 39.93; H, 5.66; N, 14.44.

1-Ethyl-2-(1-oxy-3-oxo-4,4,5,5-tetramethylimidazolin-2-yl)-3-methylimidazolium Bis(trifluoromethanesulfonyl)imide, [EMINN] $^+$ [TFSI] $^-$. Lithium bis(trifluoromethanesulfonyl)imide (181 mg, 0.52 mmol) was added to a solution of MINN (150 mg, 0.43 mmol) in hot water (2 mL). The solution was vigorously shaken in a separatory funnel and extracted with dichloromethane, dried over magnesium sulfate, and concentrated. The crude mixture was recrystallized from MeOH/ H_2O to give [EMINN] $^+$ [TFSI] $^-$ as blue platelets in 79.5% yield (188 mg, 0.34 mmol): mp 110 °C; IR (KBr) 1379, 1348, 1197 cm^{-1} ; mass spectrum (FAB, *m*-nitrobenzyl alcohol matrix) m/z 266.2 [EMINN] $^+$, ESR (CH_2Cl_2) $g = 2.0075$, $a_{\text{N}}/2 = 7.05$ G gauss. Anal. Calcd for $\text{C}_{15}\text{H}_{22}\text{N}_5\text{O}_6\text{F}_6\text{S}_2$: C, 32.97; H, 4.06; N, 12.82. Found: C, 33.27; H, 4.08; N, 12.83.

1-Ethyl-2-(1-oxy-3-oxo-4,4,5,5-tetramethylimidazolin-2-yl)-3-methylimidazolium Tetraphenylborate, [EMINN] $^+$ [BPh $_4$] $^-$. Sodium tetraphenylborate (178 mg, 0.52 mmol) was added to a solution of MINN (150 mg, 0.43 mmol) in hot water (2 mL). The solution was vigorously shaken in a separatory funnel and extracted with dichloromethane, dried over magnesium sulfate, and concentrated. The crude mixture was recrystallized from acetone/MeOH to give [EMINN] $^+$ [BPh $_4$] $^-$ as blue platelets in 83.8% yield (213 mg, 0.36 mmol): mp 167 °C; IR (KBr) 1375 cm^{-1} ; mass spectrum (FAB, *m*-nitrobenzyl alcohol matrix) m/z 266.3 [EMINN] $^+$; ESR (CH_2Cl_2) $g = 2.0075$, $a_{\text{N}}/2 = 7.06$ gauss. Anal. Calcd for $\text{C}_{37}\text{H}_{42}\text{N}_4\text{O}_2\text{B}$: C, 75.89; H, 7.23; N, 9.57. Found: C, 75.92; H, 7.20; N, 9.49.

1-Ethyl-2-(1-oxy-3-oxo-4, 4, 5, 5-tetramethylimidazolin-2-yl)-3-methylimidazolium Benzenecarboxylate, [EMINN] $^+$ [BA] $^-$. A solution of [EMINN] $^+$ [Br] $^-$ (200 mg, 0.58 mmol) in H_2O (5 mL) was passed through a column of negative ion-exchange resin (2 mL) to

give a solution of [EMINN] $^+$ [OH] $^-$. Benzoic acid (71 mg, 0.58 mmol) was then added, and the solution was stirred at 4 °C overnight. After removal of the solvent, a crude radical was purified by recrystallization from $\text{CH}_2\text{Cl}_2/\text{Et}_2\text{O}$ at –30 °C. The crystal of [EMINN] $^+$ [BA] $^-$ was obtained as blue plates in 73.3% yield (164 mg): mp 180 °C 9dec; IR (KBr) 1559 cm^{-1} ; mass spectrum (FAB, *m*-nitrobenzyl alcohol matrix) m/z 266.3 [EMINN] $^+$, ESR (H_2O) $g = 2.0073$ and $a_{\text{N}}/2 = 7.52$ gauss. Anal. Calcd for $\text{C}_{20}\text{H}_{27}\text{N}_4\text{O}_4 \cdot 0.5\text{H}_2\text{O}$: C, 60.59; H, 7.12; N, 14.13. Found: C, 60.46; H, 7.22; N, 14.14.

Bis[1-ethyl-2-(1-oxy-3-oxo-4,4,5,5-tetramethylimidazolin-2-yl)-3-methylimidazolium] 1,4-Benzenedicarboxylate, [EMINN] $^+$ $_2$ [BA $_2$] $^{2-}$. This salt was prepared in a manner similar to [EMINN] $^+$ [BA] $^-$ by using terephthalic acid, BA $_2$, in place of benzoic acid, BA $_1$. Diradical salt [EMINN] $^+$ $_2$ [BA $_2$] $^{2-}$ was crystallized from H_2O -CH $_3\text{CN}/\text{CH}_3\text{CO}_2\text{Et}$ to give blue plates in 87.9% yield: mp 159–161 °C dec; IR (KBr) 1573, 1378 cm^{-1} ; mass spectrum (FAB, *m*-nitrobenzyl alcohol matrix) m/z 266.3 [EMINN] $^+$, ESR (H_2O) $g = 2.0076$ and $a_{\text{N}}/2 = 7.49$ gauss. Anal. Calcd for $\text{C}_{34}\text{H}_{48}\text{N}_8\text{O}_8 \cdot 5\text{H}_2\text{O}$: C, 51.90; H, 7.43; N, 14.24. Found: C, 52.08; H, 7.39; N, 14.34.

Tris[1-ethyl-2-(1-oxy-3-oxo-4,4,5,5-tetramethylimidazolin-2-yl)-3-methylimidazolium] 1,3,5-Benzenetricarboxylate, [EMINN] $^+$ $_3$ [BA $_3$] $^{3-}$. This salt was prepared in a manner similar to [EMINN] $^+$ [BA] $^-$ by using trimesic acid in place of benzoic acid. Triradical salt [EMINN] $^+$ $_3$ [BA $_3$] $^{3-}$ was crystallized from H_2O -CH $_3\text{CN}/\text{CH}_3\text{CO}_2\text{Et}$ to afford blue plates in 88.8% yield (103 mg): mp 102 °C dec; IR (KBr) 1559, 1379 cm^{-1} ; mass spectrum (FAB, *m*-nitrobenzyl alcohol matrix) m/z 266.3 [EMINN] $^+$, ESR (H_2O) $g = 2.0073$ and $a_{\text{N}}/2 = 7.49$ gauss. Anal. Calcd for $\text{C}_{48}\text{H}_{69}\text{N}_{12}\text{O}_{12} \cdot 8.5\text{H}_2\text{O}$: C, 49.73; H, 7.48; N, 14.50. Found: C, 49.62; H, 7.41; N, 14.48.

1-Ethyl-2-(1-oxy-3-oxo-4,4,5,5-tetramethylimidazolin-2-yl)-3-methylimidazolium 4-(1-Ethyl-2-(1-oxy-3-oxo-4,4,5,5-tetramethylimidazolin-2-yl)benzenecarboxylate, [EMINN] $^+$ [BANN] $^-$. This salt was prepared in a manner similar to [EMINN] $^+$ [BA] $^-$ by using BANN in place of benzoic acid. Diradical salt [EMINN] $^+$ [BANN] $^-$ was crystallized from acetone/ Et_2O to afford blue plates in 51.5% yield: mp 176–177 °C dec; IR (KBr) 1589, 1370 cm^{-1} ; mass spectrum (FAB, *m*-nitrobenzyl alcohol matrix) m/z 266.3 [EMINN] $^+$, ESR (H_2O) $g = 2.0072$ and 2.0071, and $a_{\text{N}}/2 = 7.5$ and 8.1 gauss. Anal. Calcd for $\text{C}_{27}\text{H}_{38}\text{N}_6\text{O}_6 \cdot 2\text{H}_2\text{O}$: C, 56.04; H, 7.32; N, 14.52. Found: C, 56.03; H, 7.33; N, 14.47.

Acknowledgment. We are grateful to Dr. M. Minoura for assistance with the X-ray crystallography. We also thank Dr. K. Goto and Dr. M. Mishima for assistance with ESI-mass measurements and the discussion of water structure. This work was supported by a Grant-in-Aid for Scientific Research (B)(2) (No.17350070) from the Ministry of Education, Science, Sports and Culture, Japan, and by “Nanotechnology Support Project” of the Ministry of Education, Culture, Sports, Science and Technology (MEXT), Japan.

Supporting Information Available: The plots of T_1 and T_2 vs concentration (Figure S1) of all salts at 25 °C. Full crystallographic data (CCDC No. 670821, 678889, 678890, 678891, 670823, 670822, and 672372) for [EMINN] $^+$ [Br] $^-$, [EMINN] $^+$ [I] $^-$, [EMINN] $^+$ [TFSI] $^-$, [EMINN] $^+$ [BPh $_4$] $^-$, [EMINN] $^+$ [BANN] $^-$, [EMINN] $^+$ $_2$ [BA $_2$] $^{2-}$, and [EMINN] $^+$ $_3$ [BA $_3$] $^{3-}$ have been deposited at the Cambridge Crystallographic Database Center and are available on request from the Director, CCDC, 12 Union Road, Cambridge, CB2 1EZ, UK (Fax: +44-1223-336-033; Email: deposit@ccdc.cam.ac.uk or http://www.ccdc.cam.ac.uk). This material is available free of charge via the Internet at http://pubs.acs.org.

JO801657A